

Stability evaluation of shallow blocks in high and steep slope combining TLS and UAV photogrammetry

Jun-lin Chen, Hai-bo Li, Nan Jiang, Qin Chen, Yu-chuan Yang & Jia-wen Zhou

To cite this article: Jun-lin Chen, Hai-bo Li, Nan Jiang, Qin Chen, Yu-chuan Yang & Jia-wen Zhou (2025) Stability evaluation of shallow blocks in high and steep slope combining TLS and UAV photogrammetry, *Geomatics, Natural Hazards and Risk*, 16:1, 2464052, DOI: [10.1080/19475705.2025.2464052](https://doi.org/10.1080/19475705.2025.2464052)

To link to this article: <https://doi.org/10.1080/19475705.2025.2464052>



© 2025 The Author(s). Published by Informa UK Limited, trading as Taylor & Francis Group.



[View supplementary material](#)



Published online: 11 Feb 2025.



[Submit your article to this journal](#)



Article views: 308



[View related articles](#)



[View Crossmark data](#)



Stability evaluation of shallow blocks in high and steep slope combining TLS and UAV photogrammetry

Jun-lin Chen^a, Hai-bo Li^b, Nan Jiang^a, Qin Chen^b, Yu-chuan Yang^c and Jia-wen Zhou^{a,d}

^aState Key Laboratory of Hydraulics and Mountain River Engineering, Sichuan University, Chengdu, PR China; ^bCollege of Water Resource and Hydropower, Sichuan University, Chengdu, PR China; ^cPowerChina Chengdu Engineering Corporation Limited, Power Construction Corporation of China Corporation, Limited, Chengdu, PR China; ^dInstitute for Disaster Management and Reconstruction, Sichuan University-The Hong Kong Polytechnic University, Chengdu, PR China

ABSTRACT

Failure of rock slopes constitutes a prevalent geohazard inherent to transportation networks and structures situated in high and steep mountainous terrains, resulting in fatalities and infrastructural damage. This study delineates a framework for evaluating the stability of shallow blocks within an intricate alpine topography, including data acquisition, automatic discontinuity extraction and stability assessment of shallow blocks. The proposed methodology leverages composite surveys to generate high-resolution point clouds using terrestrial laser scanning (TLS) and Unmanned Aerial Vehicle (UVA), facilitating the rapid assessment of the shape, volume, and safety factor of unstable blocks by employing an auto-discontinuity extraction algorithm. In case studies, we discovered that the discontinuities orientation of natural slopes and excavated slopes has changed. This discrepancy significantly influences the instability mechanism of these slopes, leading to precise identification of falling blocks after slope excavation, which is particularly prevalent on roads and unsupported slopes. Consequently, the proposed method is of paramount significance for the assessment of slope stability during construction and offers valuable insights for the formulation of safety measures. Furthermore, its potential to facilitate rapid and accurate assessments of rock mass instability hazards and locations underscores its importance in ensuring the stability of shallow blocks in these terrains.

ARTICLE HISTORY


Received 15 November 2024
Accepted 3 February 2025

KEYWORDS

Slope stability analysis; discontinuities; high-resolution point clouds; rockfall

1. Introduction

Natural or manmade rock slope excavation are ubiquitous in civil projects such as highways and railways, dams for power production, open pits for mining, and the slope stability significantly impacts engineering progress and safety. The failure of

CONTACT Jia-wen Zhou  jwzhou@scu.edu.cn

© 2025 The Author(s). Published by Informa UK Limited, trading as Taylor & Francis Group.

This is an Open Access article distributed under the terms of the Creative Commons Attribution-NonCommercial License (<http://creativecommons.org/licenses/by-nc/4.0/>), which permits unrestricted non-commercial use, distribution, and reproduction in any medium, provided the original work is properly cited. The terms on which this article has been published allow the posting of the Accepted Manuscript in a repository by the author(s) or with their consent.

rock slopes is a natural common geohazard to transportation networks and structures in hilly and steep mountainous terrains, leading to fatalities and damage to infrastructure (Abellán et al. 2006; Lan et al. 2010; Badoux et al. 2016). Therefore, the stability of rock slopes has garnered increasing attention in both geotechnical engineering practice and academia. However, a key challenge lies in defining the appropriate analysis parameters for rock slopes with varying properties (Hoek and Bray 1981; Li et al. 2022). Over the past few decades, significant breakthroughs have been made in evaluating the instability mechanisms of engineered slopes (Markland 1972; Günther et al. 2004). In fact, the limited time and insufficient survey data of slopes have frequently forced slope stability analysis into a dilemma (Wang et al. 2023). However, emerging advanced technologies, such as unmanned aerial vehicle (UAV) photogrammetry and terrestrial laser scanning (TLS) techniques in geological surveys, have significantly improved the efficiency and comprehensiveness of acquiring survey data on slopes while enhancing the safety of investigators and reducing economic costs.

TLS generates three-dimensional (3D) point clouds from surveyed objects with high speed and accuracy (Abellán et al. 2006; Ferrero et al. 2009). In recent years, TLS has become a widely used for rock discontinuity extraction and monitoring of unstable slopes (Riquelme et al. 2014; Gigli et al. 2022), particularly for rockfall and slope instability analyses (Matasci et al. 2018; Chen et al. 2024). Furthermore, high-resolution point clouds obtained *via* TLS provide a valuable means for creating accurate 3D surfaces and digital elevation models (DEMs), aiding engineering surveys and subsequent geotechnical analyses (Li et al. 2019; Zhou et al. 2024a). Therefore, the integration of TLS with traditional geological surveys is increasingly used for geological mapping, stratigraphic modeling, extraction of discontinuities, and deformation monitoring of steep rock slopes and pit cliffs. These transitions highlight the versatility and efficacy of TLS in advancing geological and geotechnical practices.

Photogrammetry technologies have significantly improved over the past several years, with the most popular being the UAV photogrammetry. The UAV provides close-up orthophoto and oblique photographic images of the measured object from all directions and angles and performs excellently in large-scale terrain surveys. Through drone flight planning, it can adapt to more complex terrains (Damjanović et al. 2020). Similar to TLS, UAVs can also be used to predict geological disaster hazards and analyzes slope instability by extracting geological information from rock masses (Lian et al. 2020) and drawing sensitivity maps of slope rockfall hazard (Gigli et al. 2022). In addition, photogrammetry software can further convert the obtained overlapping images into point clouds, and further create a 3D model, a 3D dense point cloud, an orthophoto, and a digital surface model (DSM) (Cledat et al. 2020; Puniach et al. 2023), thereby providing reliable data for rock engineering analysis algorithms and stability analyses of blocks.

Photogrammetry technologies have significantly improved over the past several years, with the most popular being the UAV photogrammetry. The UAV provides close-up orthophoto and oblique photographic images of the measured object from all directions and angles and performs excellently in large-scale terrain surveys. Through drone flight planning, it can adapt to more complex terrains (Damjanović et al. 2020). Similar to TLS, UAVs can also be used to analyze slope instability by

extracting geological information from rock masses (Lian et al. 2020) and draw sensitivity maps of slope rockfall hazard (Gigli et al. 2022). In addition, photogrammetry software can further convert the obtained overlapping images into point clouds, and further create 3D models, 3D dense point clouds, orthophotos, and digital surface models (DSMs) (Cledat et al. 2020; Puniach et al. 2023), thereby providing reliable data for rock engineering analysis algorithms and stability analyses of blocks.

However, it is still difficult to collect effective data on high and steep slope, even if advanced measurement technologies such as TLS and UAV are used. The use of TLS and UAV will yield more comprehensive and substantial digital data, which will continue to complement traditional measurement methods in research (Šašak et al. 2019; Błaszczyk et al. 2022). Therefore, previous studies focused on the combined use of traditional technologies (Xu et al. 2023), optimization the recognition algorithm (Riquelme et al. 2014; Jaboyedoff et al. 2019; Gigli et al. 2022). An important area of study is how to interpret digital data and integrate traditional measurement methods to fully leverage the advantages of all technologies and optimize geological survey plans.

The 3D data obtained from TLS or UAV surveys contain spatial information about the slope surface. However, manually measuring structural plane information from large 3D datasets is challenging and time-consuming, and further interpretation is required to extract geological information related to the structural plane, which is known as rock discontinuity. Recent research efforts have led to the development of semi-automatic and automatic algorithms that significantly reduce the time required to extract discontinuity information from 3D data (Riquelme et al. 2014; Gigli et al. 2022; Zhou et al. 2024b). After obtaining geological information about the rock mass, including discontinuity data, kinematic analysis can be used to evaluate its stability. Kinematic analysis delineates potentially hazardous areas using the Markland test (Markland 1972) and is widely employed for the rapid assessment of slope stability (Mavrouli and Corominas 2017; Matasci et al. 2018; Chen et al. 2024). To evaluate slope stability, it is essential to carefully select relevant parameters; therefore, mutual verification between data obtained from various sources is also required.

This case study evaluates the shallow layer stability of high and steep slopes using multisource data. It fully utilizes the flexibility of UAVs to collect large-scale data in mountainous areas, while combining high-resolution point clouds scanned *via* TLS at close range to generate more accurate 3D models. After data acquisition, automatic identification algorithms were applied to extract feature information related to rock mass discontinuities. The results were cross-validated through comparison with traditional geological survey findings. Finally, to address common engineering concerns regarding surface instability, an analysis of the instability mechanisms associated with surface stability was conducted. This analysis aims to provide supportive data for engineering design consideration.

2. Background

2.1. Geo-environment

The study area, situated on the southeastern margin of the Tibetan Plateau, exhibits distinct topographical features characterized by deep valleys and undulating terrain. A

high and steep slope on the left bank of the valley, with elevations ranging from 4,400 to 4,600 (m.a.s.l.) and a slope angle of approximately 65° – 80° , is the focus of this study. The average elevation here is 2,100 m higher than that of the valley floor. The granite in this area has favorable mechanical properties for nearby engineering projects, such as earth-rock dams. A quarry, planned to exceed 300 m in height and cover an area of approximately $2.3 \times 10^5 \text{ m}^2$, has undergone multiple geological surveys. The quarry's total length is nearly 1,000 m, with the third zone, located between two gullies, being the primary area of focus for this study. Figure 1a shows an overview of the three quarry zones. The third zone is approximately 300 m in length, with its starting point at an elevation of 2,700 m. Within this area, slope dip angles gradually decrease to 35° – 45° . Figures 1b–d present typical cases of falling blocks along transportation roads and construction areas. To ensure safety in the third zone of the quarry, where excavation exceeds 300 m in height, more detailed geological slope data are required.

The shape of the quarry slope continually changed as excavation progressed. However, on-site investigations have mainly focused on sampling the surface and internal sections of the slope before excavation, which leads to significant discrepancies between survey results and the actual conditions of the excavated slope. Conducting frequent on-site investigations to match excavation progress is both time-consuming and impractical. As a result, estimating slope stability during excavation, before completing slope support measures, can only be done roughly. The lack of

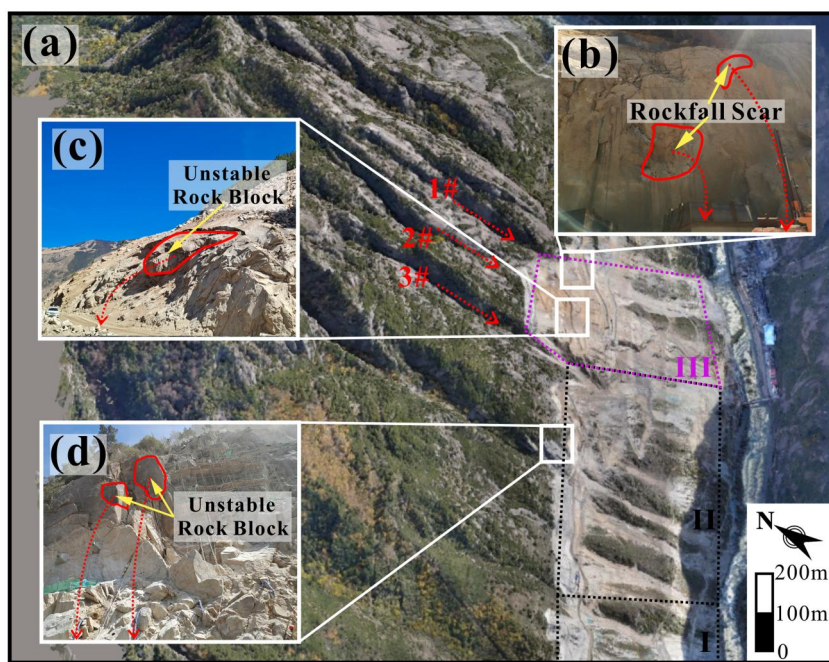


Figure 1. Rockfall hazards in the study quarry: (a) overview of the engineering area, "I", "II" and "III" are three parts of quarry, "1#", "2#" and "3#" are three gullies at the third part of quarry; (b) block detachment; (c) typically instability block around transport road; and (d) unstable blocks in the excavation area.

precise data often leads to the use of conservative estimates to ensure construction safety, potentially reducing the economic benefits of the project.

2.2. Workflow

Many facilities and transportation corridors cross mountainous areas where rockfalls cause high-frequency geological disasters. Figure 1a shows the distribution of such facilities in a typical mountainous area, where long, linear traffic routes pass through the terrain, and unstable rock masses are likely to occur intermittently along these roads. Hazardous rock masses are common during construction, and the evolving shape of the slope during excavation contributes to continuously changing threats from unstable blocks. These conditions present three primary challenges in conducting geological surveys in mountainous terrain. Firstly, the complex terrain in the alpine region made the on-site investigations exceptionally challenging. The presence of potential geological hazards such as rockfalls imposes constraints on the duration and extent of geological surveys. Consequently, traditional on-site surveys, including geological drilling, core sampling, discontinuity measurement, and mechanical performance testing, need to be done as soon as possible. This would magnify the second disadvantage, there may have been many blind spots during data collection. The noncontact measurement method is an effective approach for rapidly obtaining large-scale terrain information, but in the rugged alpine terrain complicates data collection, resulting in several blind spots using only one method. Finally, large-scale data processing is a major challenge. Although long-line construction areas may not be extensive, mountainous regions prone to rockfalls often have widely distributed dangerous rock blocks that threaten transportation routes. This requires comprehensive analysis of the entire mountainous area, which is time-consuming. To address this challenge, TLS and UAV photogrammetry measurement technologies offer more accurate, high-frequency methods for collecting geological slope data, which are crucial for slope stability analysis. A schematic representation of this approach is shown in Figure 2, outlining three key steps: high-resolution point cloud generation, discontinuity extraction, and slope stability analysis.

3. Methodology

3.1. High-resolution point clouds generations

Point cloud data is a common format for describing slope surface topography. However, both TLS and UAV measurement systems have limitations when applied to rugged alpine terrain, as shown in Figure 3e. The uneven terrain across the slope often results in data shadowing, making it difficult to capture complete coverage. While TLS is efficient and accurate for acquiring geological information from slope surfaces, it faces significant challenges in steep and deep canyons due to view occlusion. Even with multiple scanning locations, the presence of rugged terrain can make it difficult to overcome this issue. In contrast, UAVs provide a practical solution, and UAV photogrammetry offers flexible operation, reducing the cost and hazards associated with fieldwork, while significantly enhancing the speed and quality of data

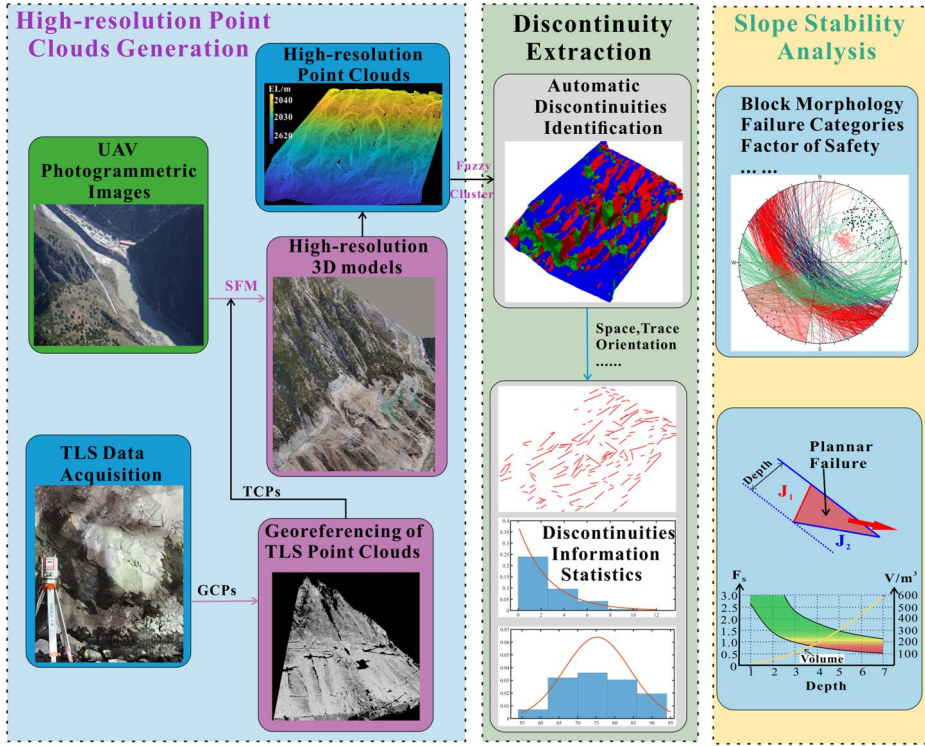


Figure 2. Schematic workflow of the combined use of TLS and UAV photogrammetry for shallow layer stability analysis of the rugged alpine topography.

acquisition. Unlike TLS, which relies on laser scanning, UAVs equipped with high-definition cameras capture aerial photographs. By executing carefully planned flight paths and capturing overlapping images from various directions, UAVs can generate large-scale, high-precision point-cloud data of slopes using real-time kinematics or other correction techniques. The precision of these point clouds depends on the number of ground control points (GCPs) measured (Siqueira et al. 2019; Cabo et al. 2021), and the point clouds with average point spacing ranging from 0.1 to 0.5 m often are obtained. However, due to limited resources, quarries in Figure 1a often have sparsely arranged GCPs, which may lead to point cloud data that does not meet the requirements for detailed slope stability analysis. To address this, we employed joint methods to minimize data shadowing while ensuring the overall point cloud data high-precision.

A RIEGL VZ2000i scanner was used to obtain high-precision local 3D spatial point clouds (Copyright RIEGL Laser Measurement Systems GmbH 2024). These data not only provide high-density and high-precision point clouds but also serve as control points for dealing with UAV photogrammetric images. Unlike using TLS alone to obtain point clouds, which requires the deployment of multiple stations to avoid scanning line-of-sight obstructions, joint measurements involving both TLS and UAV technology offer greater flexibility in the station layout. Additionally, Global Navigation Satellite System (GNSS) was employed to measure the geographic coordinates of each scanning station and feature points along the route, serving as ground

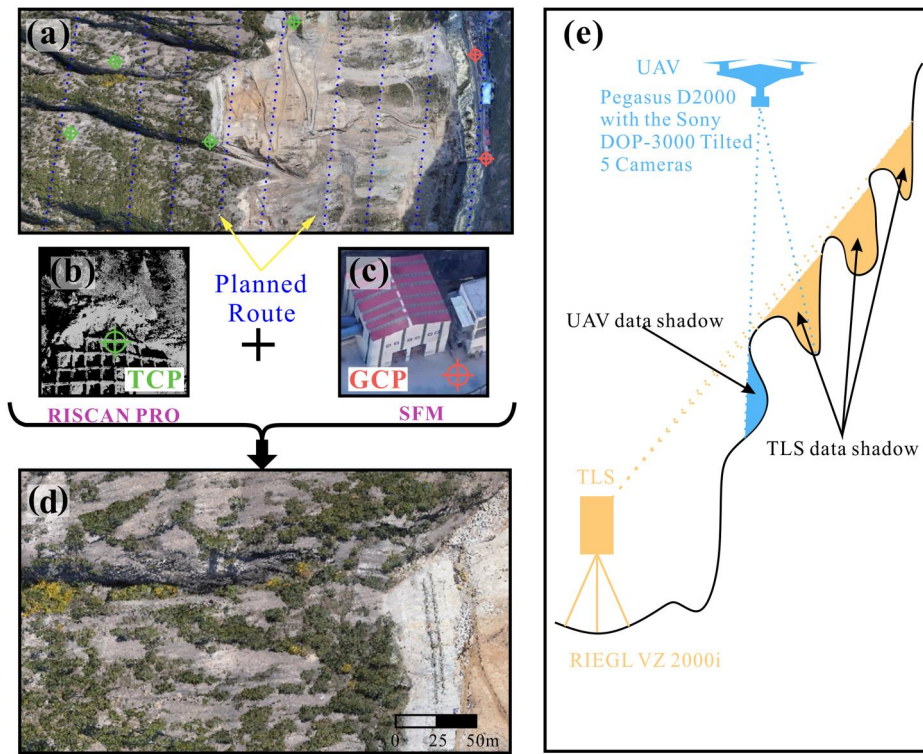


Figure 3. The TLS–UAV method of investigation: (a) route planning and control points layout; (b) selected points in TLS point cloud as control points; (c) ground control points, (d) high-resolution true-coloured point cloud and (e) viewing geometry and data coverage obtained *via* TLS and UAV from single positions in rugged terrain.

verification points for point clouds registration. This integrated approach enhanced the efficiency and accuracy of data collection for slope analysis. As shown in Figure 3e, the UAV photography in this project utilizes a Feima robotics D2000 UAV and a Sony DOP-3000 tilt photography camera, and the flight altitude of approximately 319 m. We chose to fix the height relative to the ground to ensure that the resolution of all images is close to 5 cm/pixel, which is about 300 m in this case according to the intrinsics of the camera. And for defining UAV routes, the longitudinal and lateral overlap rates are usually no less than 70% and 60%, while the longitudinal and lateral overlap rates of 80% and 65% are the recommended parameters for D2000 drone, which are integrated into the aerial photogrammetry software. Initial terrain data for the quarry slopes was collected in November 2022 and the second collection taking place in April 2023. Two collection times coincided with the completion of the first and second stages of quarry excavation.

Figure 3 illustrates a combined method that integrates the strengths of both TLS and UAV technologies for data acquisition. The fusion point clouds were generated using the RiSCAN PRO software package (<http://www.riegl.com/index.php?id=221>), which performs denoising, merging, and referencing the GCPs. This process results in point clouds with an average point spacing of 0.005–0.01 m. Specific feature points,

selected from the point clouds, are designated as TLS control points (TCPs), as shown in [Figure 3b](#). These TCPs, along with the GCPs, are used as control points in the processing of UAV images, ensuring the generation of high-quality 3D models through structure from motion (SfM) method. The outputs include true-color 3D point clouds (in [Figure 3d](#)), orthophoto data, and digital elevation models (DEMs). In this method, TLS is renowned for its high accuracy, particularly for closed-range repeated scans. By using the registered TLS point-cloud coordinates as TCPs, sparse GCPs can be transformed into densely arranged ones, improving the accuracy of the UAV data (Jiang et al. 2022). The TLS-UAV joint technology combines the precision of TLS with the flexibility of UAVs, resulting in faster data acquisition, enhanced coverage, and maintaining the point clouds with an average point spacing of 0.01–0.05 m. These TLS-UAV point clouds form the basis for generating comprehensive 3D models or DEMs of the rock masses. Furthermore, the integrated TLS-UAV data facilitate the recognition and extraction of discontinuities and other geological features, providing the necessary inputs for slope stability analysis.

3.2. Automatic discontinuity extraction

TLS-UAV data are so vast and time-consuming to process that one must resort to automated algorithms. The main objective of automatic algorithms is to obtain geological information on discontinuities, including weak structural planes, fissure joints, and outcrops. Clustering algorithms are used to differentiate point clouds corresponding to different objects, such as joint sets and vegetation, based on differential measurement indicators. Segmentation algorithms are then applied to isolate the targeted discontinuities from the point clouds. These algorithms can run simultaneously to optimize the process. Joint measurement technology provides multiple data types that are suitable for various discontinuity extraction methods. In this case, a method based on point-cloud data is introduced to extract discontinuities (Zhou et al. 2024b). This approach leverages fuzzy clustering and segmentation algorithms to effectively extract the desired geological information from the point clouds. The extraction of discontinuities from point-cloud data involves several steps. An overview of this process is as follows.

1. **Vegetation Removal:** Vegetation can interfere with the accuracy of the algorithms and lead to unreliable results. To address this, the RGB values of vegetation and rock are utilized by software like RiSCAN PRO to filter out the vegetation. A terrain-filtering function is then applied to remove any remaining vegetation. [Figure 4a](#) shows the processed TLS-UAV point cloud used for extracting discontinuities.
2. **Triangulation:** The next step involves using a triangulation algorithm to approximate the structural surface linearly. This process helps in representing the overall shape of the slope and its structural features. [Figure 4b](#) illustrates the Triangulated Irregular Network (TIN) models, with the normal vectors of the triangular patches being calculated during this step.
3. **Clustering and Grouping:** The normal vectors of the triangular patches represent the orientation of the corresponding structural planes. Different sets of

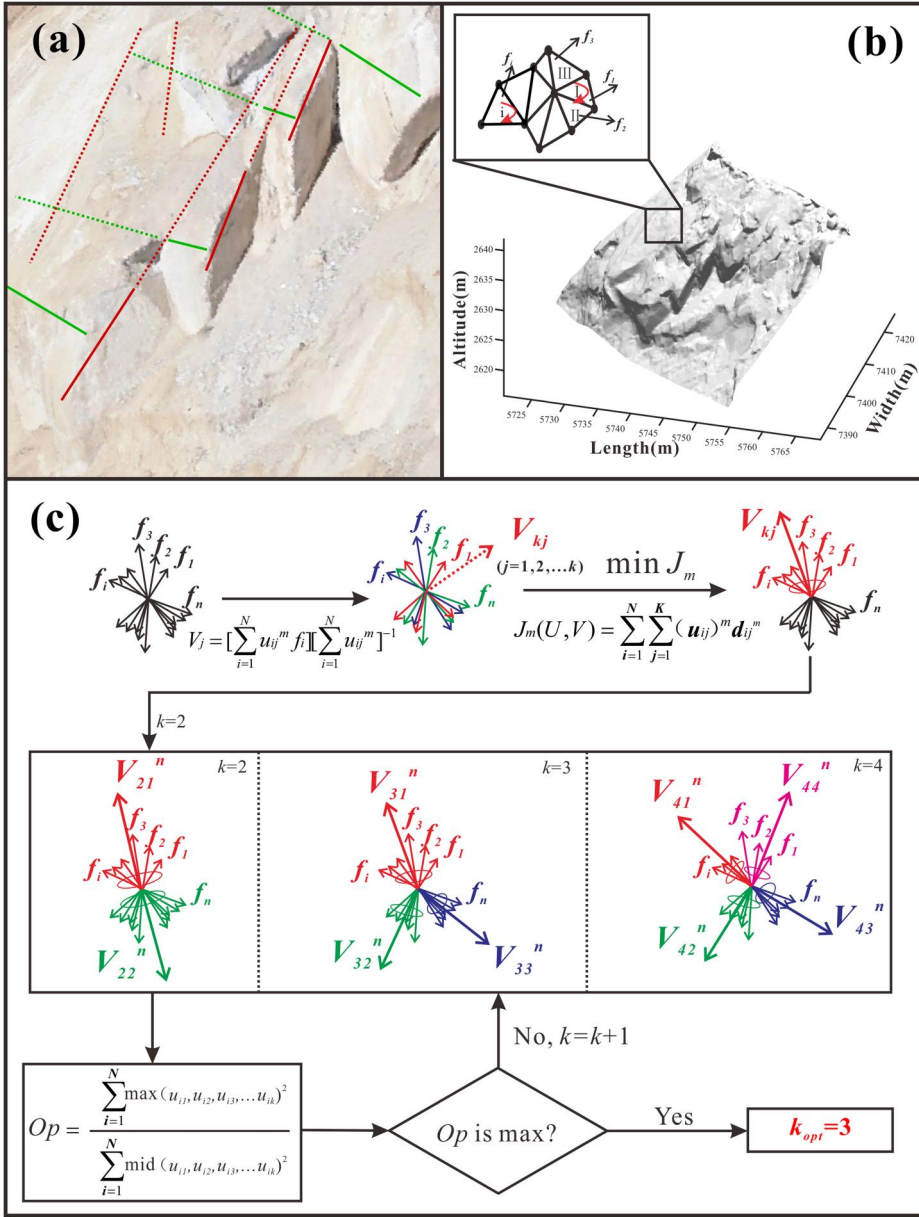


Figure 4. Automatic discontinuity extraction of optimized fuzzy clustering: (a) high-resolution true-coloured point cloud of the rock slope; (b) TIN (triangulated irregular network) models; (c) a workflow of the optimized fuzzy cluster algorithm.

discontinuities show significant variations in their characteristics. In our method, the cosine value of the angle between the normal vectors of the fitting planes is used as a differential measurement indicator for fuzzy clustering. Discontinuities with similar characteristics are grouped together. The optimal number of clusters is selected by continuously calculating the Op (optimality parameter) for different

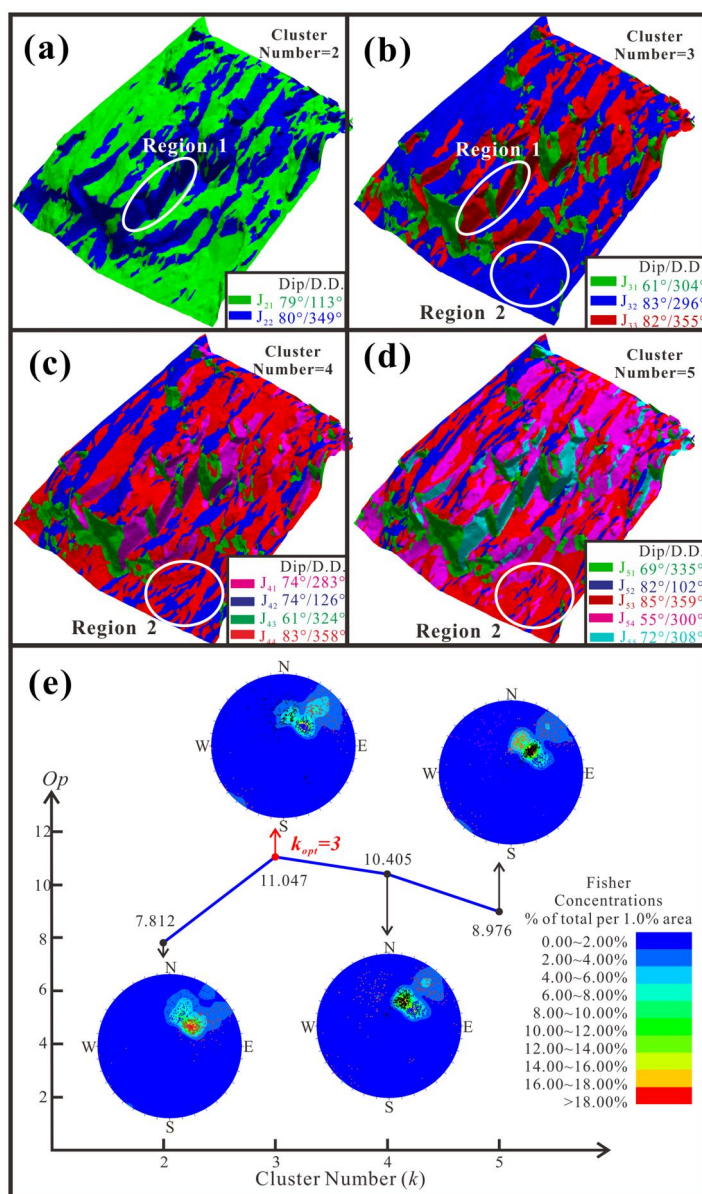


Figure 5. Result of automatic discontinuity extraction with different cluster numbers: (a) cluster number is 2; (b) cluster number is 3; (c) cluster number is 4 (d) cluster number is 5; and (e) the Op of different cluster numbers and stereographic projection chart.

cluster counts (Figure 4c). The maximum Op value indicates the appropriate clustering solution (Figure 5e).

4. Separation of Discontinuities: The fuzzy clustering algorithm divides the point cloud into multiple joint sets, grouping points that belong to the same structural plane. A region-growing algorithm is then applied to separate each discontinuity from the point cloud. Figures 5a–d show the results of discontinuity

identification with different clustering numbers (ranging from 2 to 5). These results confirm that the maximum Op corresponds to the correct clustering solution. When the number of clusters is fewer than three, such as in region 1, the clustering results are inconsistent with the actual discontinuities. When the number of clusters exceeds three, such as four or five, such as in region 2, the clustering results become sensitive to fluctuations, causing discontinuities to be over-clustered into several groups.

5. **Extraction of Discontinuity Information:** After separating the discontinuities, further analysis is performed using their spatial geometric relationships to extract key information, such as occurrence, spacing, and trace length. Figure 6 presents the discontinuity data for the area shown in Figure 4, Figure 6a shows the trace of discontinuity sets; Figure 6b shows discontinuity sets in Lower Hemisphere Projection; and Figure 6c shows trace statistics chart of discontinuity sets. These data offer valuable insights into the characteristics and distribution patterns of discontinuities within the slope.

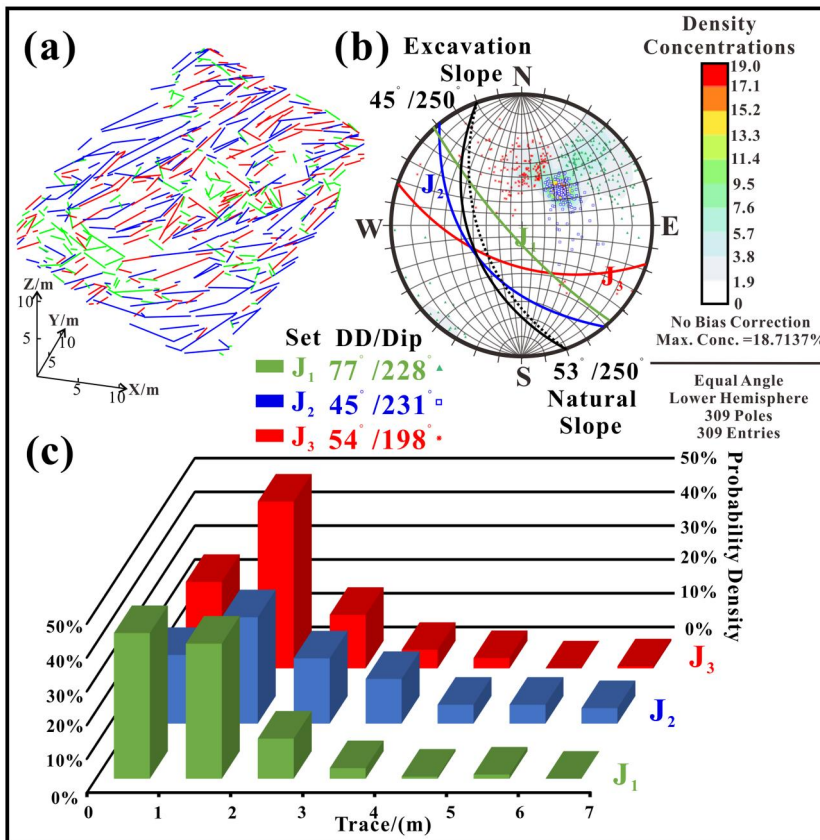


Figure 6. Result of automatic discontinuity extraction of slope Figure 3c: (a) the trace of discontinuity sets; (b) discontinuity sets in lower Hemisphere projection; and (c) trace statistics chart of discontinuity sets.

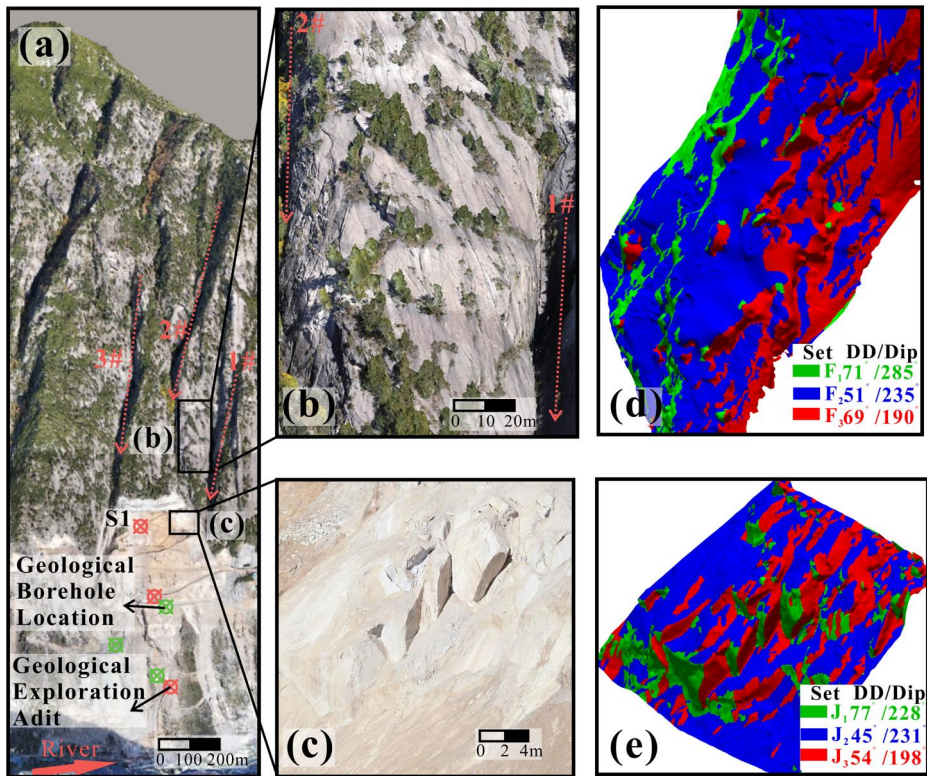


Figure 7. Geo-environment and filed investigation in the study quarry: (a) the location of on-site survey; (b) an upper natural slope of excavation area; (c) a part of typical excavation slope; (d) automatic discontinuity extraction of slope b; and (e) automatic discontinuity extraction of slope c.

By following these steps, the algorithm effectively extracts and characterizes the discontinuities in the point-cloud data, contributing to a better understanding of the geological features of the rock slope.

3.3. Field investigation

While existing digital measurement technologies have enhanced the efficiency of certain geological survey tasks, it is imperative to substantiate the efficacy of digital measurement methods by comparing them with traditional measurement techniques. Otherwise, it would be challenging to determine the credibility of the results obtained using digital measurement technology. Figure 7a is the processed results as a 3D model of the third quarry, and the locations of the adits and boreholes are shown here. The discontinuities within the slope are a crucial factor in determining shallow stability. Three distinct sets of discontinuities (g1, g2, and g3) were observed in the S1 adit, and their specific occurrences and depths are listed in Table 1. The area for automatic discontinuity extraction in Figure 6 is close to S1, so it is also included in Table 1. Currently, the excavation of the quarry towards the lower portion of the S1 adit significantly impacts the shallow stability of the excavated slope owing to the presence of two sets of shallow discontinuities, g1 and g2. But g3 still has a depth of

Table 1. Orientation of identified discontinuity sets by using automatic discontinuities identification method and traditional geological survey results.

Similarity	Automatic discontinuities identification method [mean dip angle / mean dip direction]	Field geological survey results [mean dip angle / mean dip direction] (Depth)
Similar	J ₁ 45° / 231°	g ₁ 45° / 225° (>10 m)
Similar	J ₂ 77° / 228°	g ₂ ~90° / 230° (>50 m)
Dissimilar	J ₃ 54° / 198°	g ₃ 80° / 170° (>70 m)

Table 2. The parameters came from on-site shear tests and analogical reasoning on similar engineering projects.

Type	Parameters of discontinuities filled soil-rock-mixture			
	Temporary slope		Ultimate slope	
	Internal friction angle (°)	Cohesion (MPa)	Internal friction angle (°)	Cohesion (MPa)
B1 (debris)	22-27	0.10–0.15	22	0
B2 (debris and a few soil)	19-22	0.05–0.10	19	0
B3 (soil and a few debris)	14-19	0.002–0.05	14	0
B4 (soil)	10-14	0.001–0.002	11	0

more than 20 m, it may have contributed to the continuous block detachment at the same location on the slope surface and play an important role in the deep stability analysis. At the same time, the two different results of discontinuity extraction also indicate the variability of the slope stability during different excavation stages. On-site investigations revealed that the discontinuities were filled, and the presence of fillers leads to variations in the stability of shallow rock blocks, and the low cohesion and shear strength of the fillers pose a high hazard of slope failure. In addition, the strength indicators of the discontinuities were extracted from the mechanical property tests, as listed in Table 2.

4. Results

4.1. Stability analysis of natural slope

To identify the factors contributing to surface instability, this case study focuses on two specific areas: one is the natural slope in Figure 7b and the automatic discontinuity extraction result shown in Figure 7d. The other is the excavation slope in Figure 7c and the automatic discontinuity extraction result shown in Figure 7e, with the processing shown in Figures 4–6 mentioned in Section 3.2. Kinematic analysis, a rapid method for identifying potential failure models of rock slopes, is employed to intuitively evaluate the stability of blocks defined by discontinuities, in combination with stereographic projections. Discontinuities are potential failure planes, and their orientation relative to the slope orientation results in three primary types of mechanisms: toppling (includes flexural toppling and direct toppling), planar sliding, and wedge sliding. Figure 8a displays the discontinuity information and stability analysis for the area shown in Figure 7b. The analysis revealed that the natural slope consists of three connective discontinuity sets: two nearly perpendicular sets (F1 and F2), and one inclined set (F3), with F3 representing the average slope orientation. The rock mass intersected by these three discontinuity sets shows a tendency for wedge sliding,

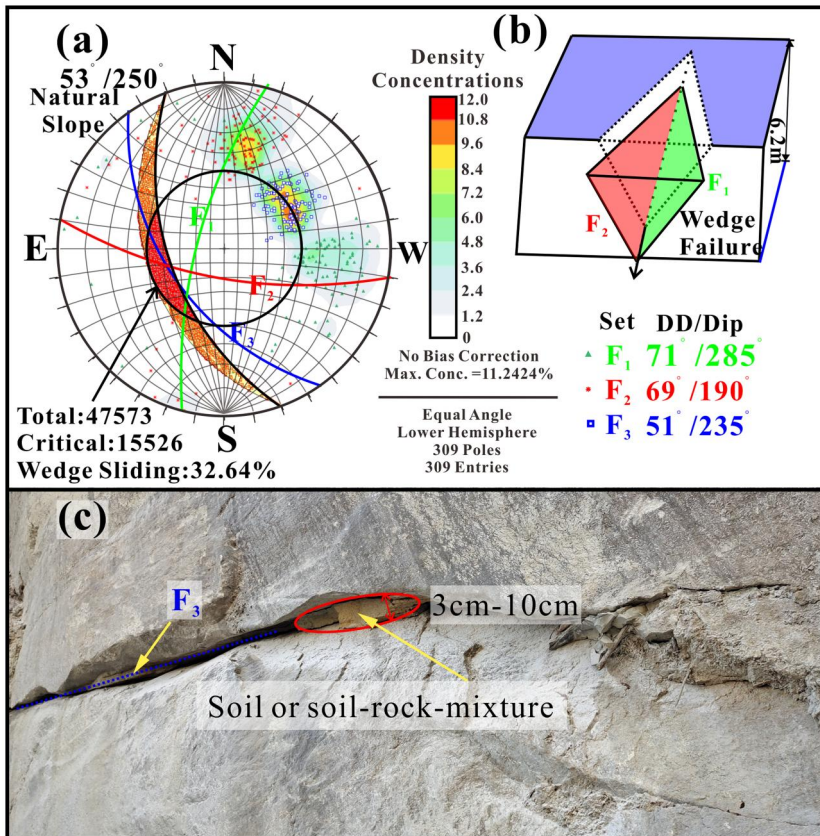


Figure 8. Result of automatic discontinuity extraction: (a) discontinuity sets in lower Hemisphere projection and kinematic analysis with friction 40° ; (b) wedge sliding with discontinuity sets F_1 and F_2 ; and (c) soil and rock debris mixture filled.

as illustrated in Figure 8b. However, the intersection between F_1 and F_2 occurs at a dip angle of approximately 29° within the slope (which has a dip angle of 53° and dip direction angle 250°). As shown in Figure 8a, considering wedge blocks by crossing all discontinuities, 32.64% of the wedge blocks will slide, compared to less than 10% without F_3 .

Additionally, the on-site photographs in Figure 8c show that F_3 was filled with soil, with an aperture width ranging from 3 to 10 cm, which significantly reduces the stability of the wedge block. To measure the actual spacing between these discontinuities, which have relatively uniform spacing, an area-weighted method was employed. Figure 9a presents the manually measured results in a 3D model, which aligns closely with the average distance of 6.2 m obtained from the statistical histogram in Figure 9c. There is a high probability of small-volume wedge blocks occurring during excavation caused by the almost fully connected discontinuity sets F_1 and F_2 . And the shallow instability of the natural slope is primarily attributed to wedge sliding also caused by the presence of F_1 and F_2 . The safety factor of the slope is influenced by F_3 and the dip angle of the topographic surface. This instability is most likely to occur in areas with significant topographic fluctuations and near gullies.

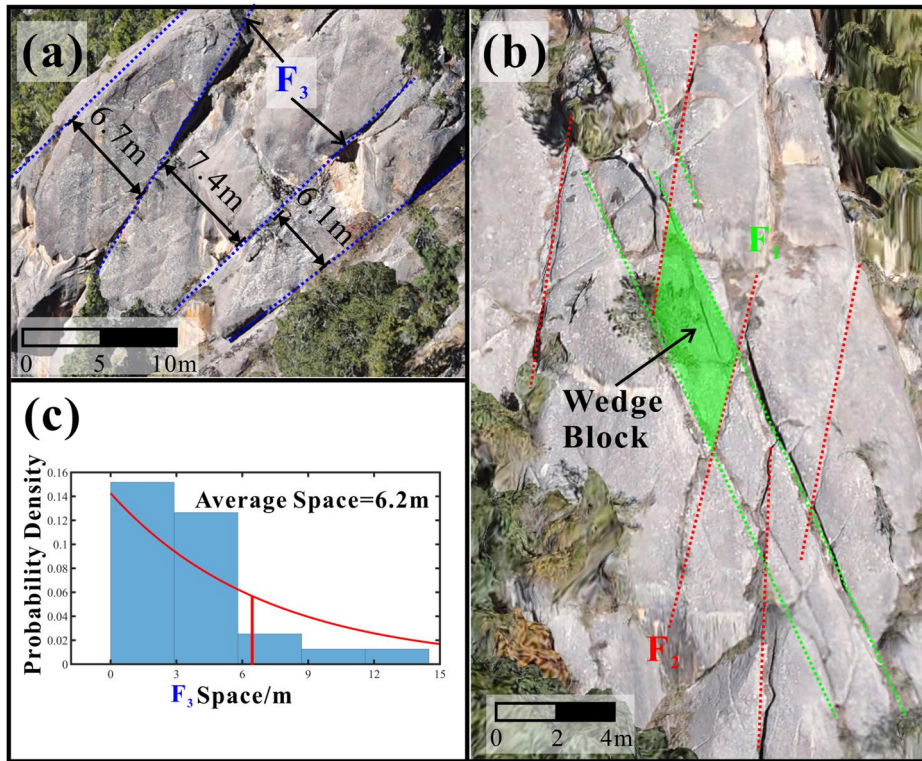


Figure 9. Analysis of wedge block size: (a) the measurement of F_3 space in 3D model (b) the measurement of F_3 space by manual method and (c) the measurement of F_3 space by auto discontinuity identification.

While on-site investigations could only reach areas near the work zone, two obvious hazardous blocks were identified in the third quarry, as shown in Figures 10a and c. The block in Figure 10b is located directly above the construction area, while the block in Figure 10c is situated at the end of gully 1# in Figure 7a, an area with previous rockfall incidents. Figures 10d and e show the kinematic analysis results for both blocks, indicating potential instability. Both blocks' stability is controlled by fractures F1 and F2, consistent with the analysis results shown in Figure 8a. Although the block in Figure 10c is closer to the construction area, it poses a lower hazard, as it is supported by plants, which further mitigate its hazard. The block in Figure 10b represents the most hazardous to machinery and workers, and a passive rockfall protection net has been installed at the upper edge of the construction zone.

4.2. Instability mechanism analysis of shallow blocks

The automatic discontinuities extraction in Figure 6 were visibly exposed during the excavation, and a geological exploration adit was located nearby. Table 1 compares the results of automatic discontinuity extraction with the findings from the adit. Discontinuity sets g1 and g2 were already observed, but g3 discovered at the deepest point, has not yet been exposed in the excavation slope. Furthermore, when

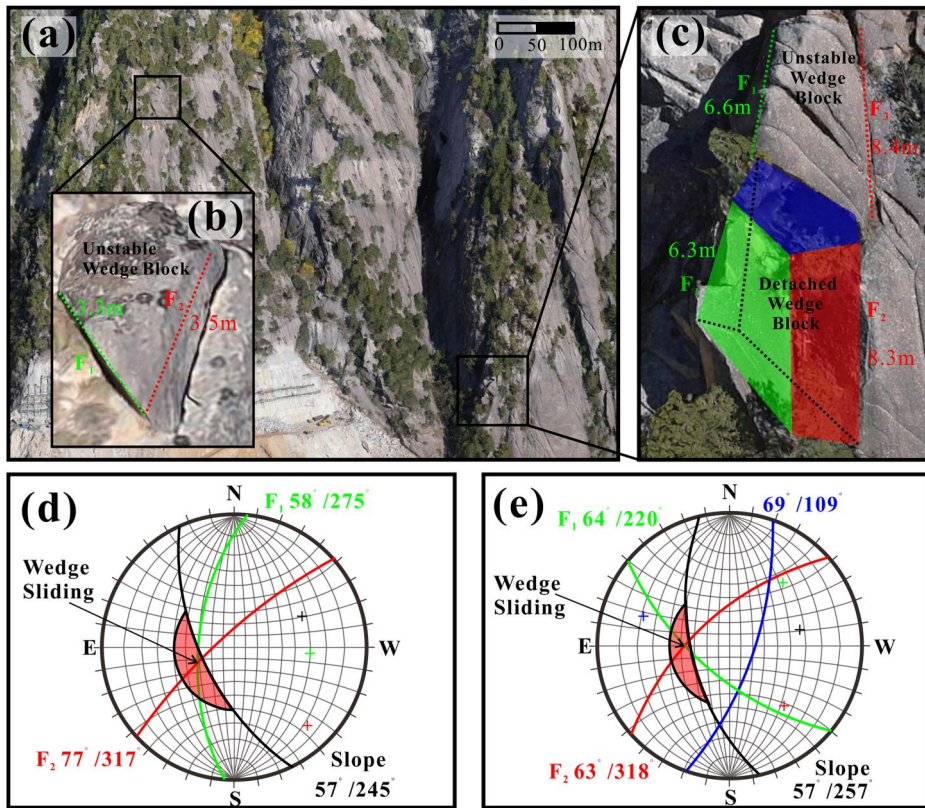


Figure 10. Dangerous blocks and rockfall investigation of environment slope: (a) the direct on-site investigation area; (b) unstable wedge block controlled by F_1 and F_2 in environment slope; (c) rockfall scar and unstable wedge block also controlled by F_1 and F_2 ; (d) kinematic analysis diagram of block (b) with friction 40° ; and (e) kinematic analysis diagram of block (c) with friction 40° .

comparing the statistical results of discontinuities in the natural slopes with those extraction result in the excavation, significant changes in the dip angles and directions were observed. This alteration suggests a shift in the instability mechanisms. The excavated slope features two discontinuity sets (J1 and J3) and one slope surface (J2), as shown in Figure 6. Unlike the shallow instability mechanism observed in the natural slope, the excavated slope is dominated by planar sliding. Figure 11 illustrates four potential failure models. The excavation of the slope reduced the depth of F3 from the slope surface (from 1–6 m), resulting in a uniform slope angle of 45° . As a result, F1 and F2 form wedges that are less prone slide but more inclined to slicing the slope into smaller rock blocks. The automatic discontinuity extraction set J2 aligns with F3, indicating that models 1.a and 1.b share the same instability mechanism. Model 2 involves planar sliding of rock blocks cut by set J1, with smaller rock blocks than those in model 1. Furthermore, considering the influence of horizontal roads, the shape of the rock blocks in model 3 aligns with that of model 2, suggesting more hazardous of instability near the road after excavation. Additionally, the blocks on the slope surface are fragmented into smaller wedges, which reduces slope stability. Deeper gullies indicate that the influence of sets F1 and F2 extends deeper than

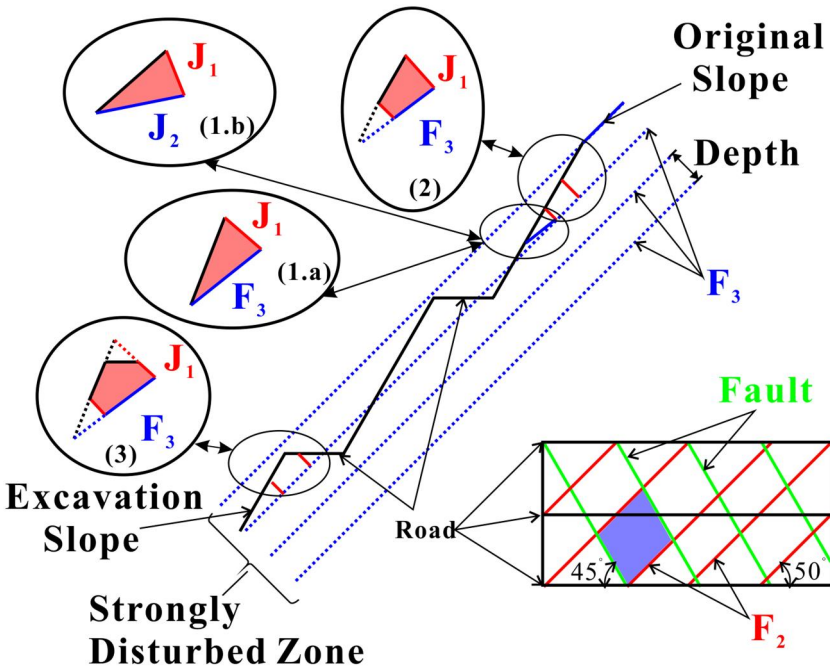


Figure 11. Block shape and failure categories analysis.

initially anticipated as shown in Figure 9b. Even if loose blocks are removed from the surface after excavation, the hazard of large wedge instability on the newly excavated slope surface cannot be ruled out.

The unstable volume of rock blocks is a critical factor in analyzing shallow slope failure. This volume is closely linked to the depth of instability, both of which influence the difficulty of preventing rockfalls based on the failure location. Since all three instability mechanisms are planar sliding, the unstable volume for models 1 and 2 can be estimated based on failure depth, as shown in Figures 12a and 13a. Discontinuity analysis in Figure 9c indicates that the spacing of F3 is approximately 6.2 m. Considering the impact of excavation, the failure depth for model 1 is estimated to range between 1–7 m. Although models 1.a and 1.b are slightly different due to the association of set J3 and F3, the failure depth and volume for model 1.b are slightly smaller than those of model 1.a as shown in Figure 11. Nevertheless, both models tend to exhibit large-volume instability, while shallower blocks remain stable due to the presence of cohesion. The calculation of the block safety factor F_s considers the presence of filling materials between discontinuities during excavation and the calculation form is,

$$F_s = T / G \sin \theta \quad (1)$$

Where T is the shear strength of the discontinuity, G is the gravitational force of a block, and θ is the dip angle of the discontinuity.

The shear strength of the discontinuity was calculated using the Mohr-Coulomb criterion and the calculation form is,

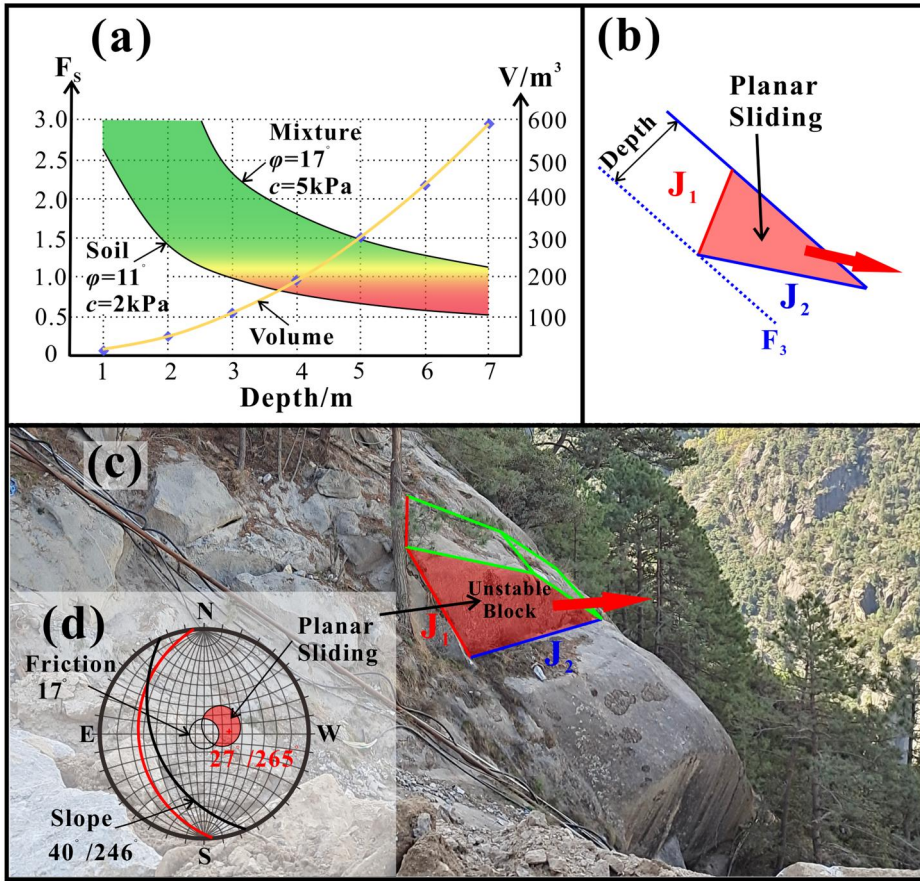


Figure 12. Volume and factor of safety estimation for model 1 in Figure 9: (a) calculation result diagram; (b) block instability shape; (c) typical on-site cases; and (d) kinematic analysis diagram.

$$T = c + G \cos \theta \tan \varphi \quad (2)$$

Where c is the cohesion, φ is internal friction angle.

And the most common filling materials for unfinished slopes are soil or soil-rock mixtures. Referring to the shear strength parameters in Table 2 from geological surveys, we chose an internal friction angle of 11° and a cohesion of 2 kPa, i.e. the discontinuity is completely filled with soil, as the lower limit of the calculation, and an internal friction angle of 17° and a cohesion of 5 kPa, i.e. the discontinuity is filled with soil-rock mixture, as the upper limit of the calculation, and we computed the law of the transformation of the coefficient of safety of the blocks with respect to the depth, as shown in Figures 12a and 13a.

A typical instability mechanism is shown in Figure 12b, with its stereographic projection analysis in Figures 12d and 13d. Due to the absence of cohesion in the kinematic analysis, a friction circle was set based on a friction angle of 17° for the filling materials with soil-rock-mixture. The calculated safety factor Fos , which considers the stability of blocks with filling materials, is only applicable to temporary slopes that have not yet been fully excavated.

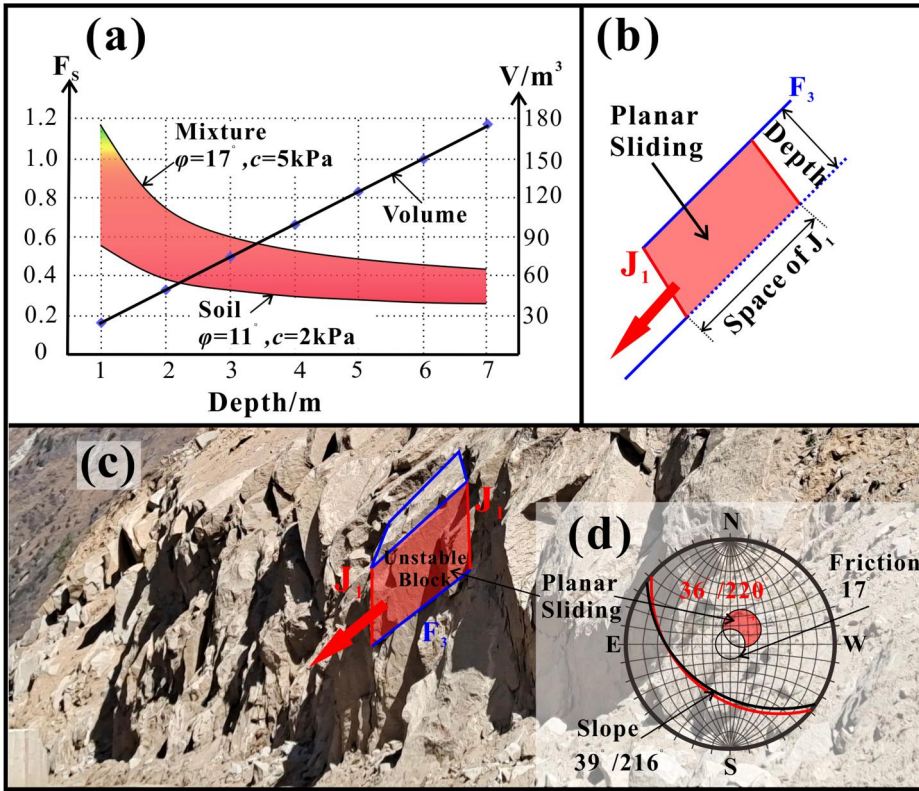


Figure 13. Volume and factor of safety estimation for model 2 in Figure 9: (a) calculation result diagram; (b) block instability shape; (c) typical on-site cases; and (d) kinematic analysis diagram.

The instability in model 1 is closely related to the persistence of the trailing-edge tensile discontinuity J_1 , as shown in Figure 12c. According to the automatic discontinuity extraction results, the exposure length of J_1 suggests that the occurrence of such blocks is relatively unlikely. The instability calculation for model 2, shown in Figure 13b, indicates that its block safety factor is much lower than that of model 1 and is associated with a smaller unstable volume. As shown in Figure 13c, the instability blocks in model 2 are more likely during excavation, especially on temporary roads used for stone transportation. Due to model 2's tendency for smaller failure depths, the requirement for the continuity of the trailing-edge tensile fracture surface J_1 is not as high, leading to a higher likelihood of rockfall issues. These blocks pose significant hazard, as they are transported over long distances, potentially causing severe damage or even loss of life due to their fall height.

4.3. Stability analysis of excavated slope and support design

The instability mechanism analysis focuses on the excavation area around the road, where discontinuities are fully exposed, as shown in Figure 7c. The result of the automatic discontinuity extraction is presented in Figure 7e. Figure 14a is an excavated slope, and Figure 14b illustrates the fissure-filled soil encountered during the excavation, further indicating that the rock mass quality at the failure site was relatively

poor. Based on an analysis of block shapes, this detachment is classified under model 3 (in Figure 11), with a failure depth of approximately 5.5 m and a volume of about 600 m^3 . Figure 14d shows the kinematic analysis diagram. The volume of detached block, calculated using model 1 (in Figure 11) with a depth of 5.5 m, was estimated at 360 m^3 , which is smaller than the actual volume of detached block. The high-quality 3D model generated through the joint method also helped measure the volume of detached block (Figure 14c). The measurement results indicated that the failure site was composed of a wedge formed by discontinuities P1, P3, and P4, contributing 360 m^3 . Additionally, 240 m^3 was provided by the blocks formed by P1, P2, and P4. The increase in volume of detached block was likely due to the strong cutting of sets F1 and F2. Post-investigation showed that the instability was primarily caused by the fissure-filled between the block and P4, where insufficient support work had been carried out.

The instability mechanism analysis indicates that the instability of excavation slopes is predominantly caused by falling blocks with a depth of less than 7 m. These blocks typically have volumes between $100\text{--}200 \text{ m}^3$. Due to the prominent rockfall issue on slopes, an anchor rods system in a staggered configuration at depths of 6 m and 9 m was designed. This shallow support system is intended to ensure the safe excavation of slope

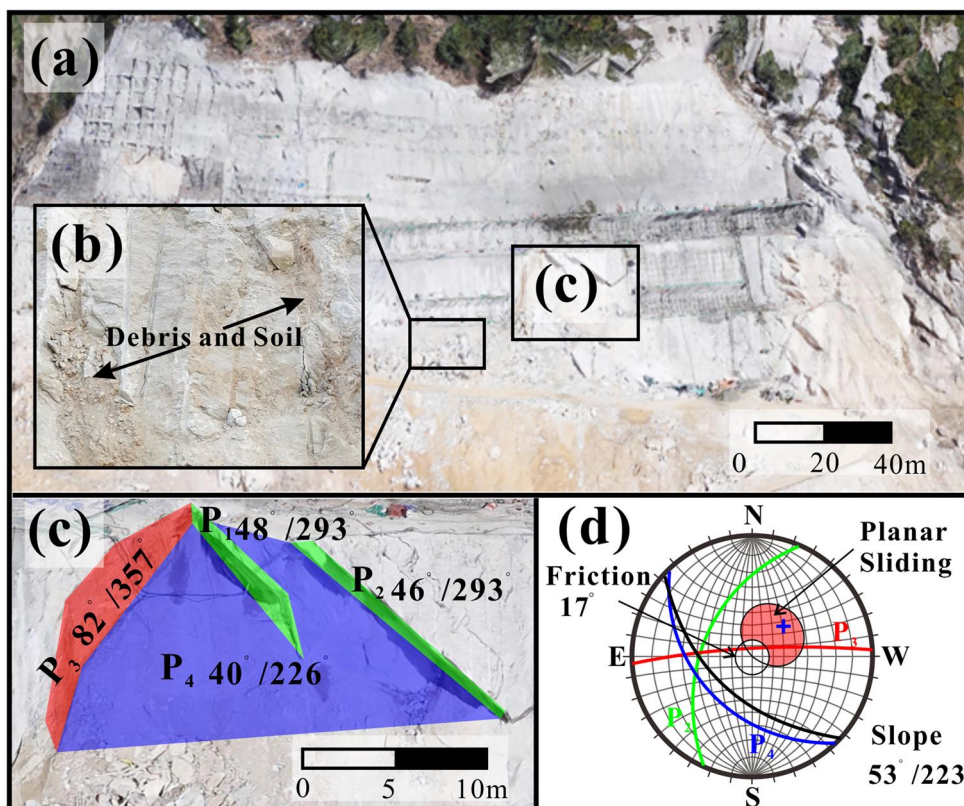


Figure 14. Failure case at excavation slope: (a) the excavation progress at the block detached, (b) the discontinuity in the unstable area, (c) the block morphological parameters, and (d) the kinematic analysis diagram.

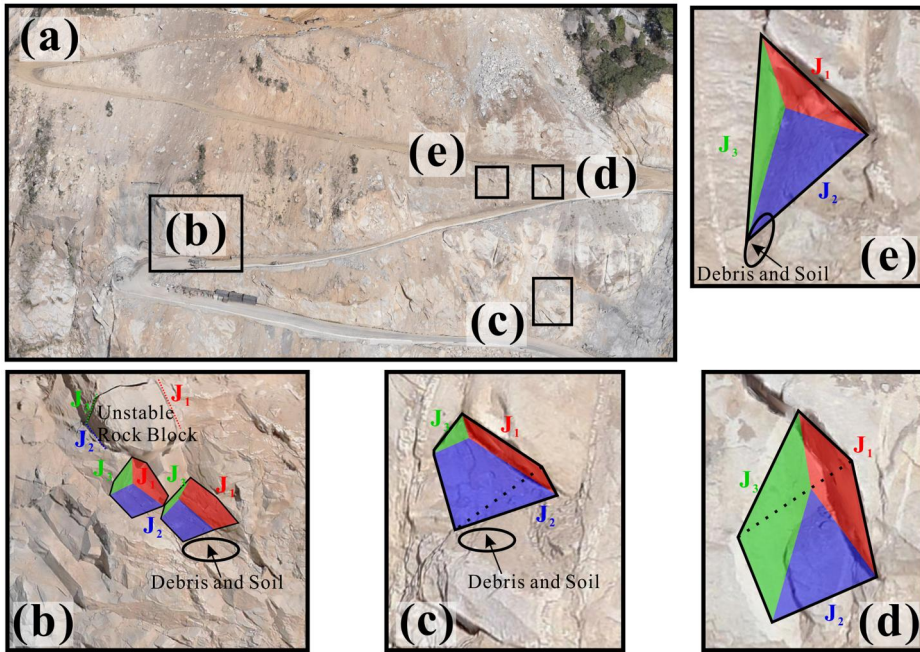


Figure 15. Failure cases at transportation corridors: (a) the transportation road of stone in the third quarry; (b), (c), (d) and (e) the rockfall scar at the excavation slope of transportation corridors.

steps and prevent potential instability of surface blocks. It guarantees that all currently exposed potentially unstable blocks are in a stable state. Figure 15 depicts the block detachments around transportation roads, Figure 15a is the transportation road of stone in the third quarry, b, c, d and e are the rockfall scar at the excavation slope of transportation corridors. The falling of unstable blocks is closely related to fissure-filled zones, with the filling material being a key factor influencing block stability. The support work and rockfall protection for excavation slopes can be optimized based on this feature. Due to the small volume of these blocks, potential unstable blocks are removed from unsupported road slopes to ensure transportation safety.

5. Discussion

A significant challenge in evaluating slope stability is the limited availability of geological data to provide comprehensive slope conditions. In contrast to simply merging the point clouds obtained from UAV and TLS, the joint approach enhances the resolution of point clouds generated by UAV and significantly reduces the overall data acquisition time. The TLS provides high resolution point clouds, particularly for selected control points (e.g. corner points of structures shown in Figure 2b), which are then used as TCPs for UAV modeling. In this study, the resolution of the final generated point cloud can reach up to 0.01 m when high-quality images are used. The accuracy of the selected TCPs can be affected when they do not correspond precisely with the image, leading to a decrease in the resolution of the final point cloud to 0.05 m, particularly for points distant from the GCP and TCP. The UAV primarily

captures the majority of area, the resolution of TLS-UAV point clouds typically ranges from 0.01 to 0.05 m, which is adequate for the automatic discontinuity extraction of the primary discontinuities of the slope.

Geological information is not easily available most of the time, resulting in a lack of a complete slope analysis. Usually, the available information is limited to surface observations and a few boreholes, which may not capture the complexity and variability of rock masses and their discontinuities. While the TLS-UAV method effectively reduces data gaps in point clouds, the impact of vegetation on discontinuity extraction remains significant. On one hand, 3D models generated by UAV photogrammetry often distort the vegetation and rock surfaces making it difficult to remove vegetation (Siqueira et al. 2019; Cabo et al. 2021). On the hand, vegetation interferes with TLS laser radiation, causing TLS to collect point cloud data of the vegetation rather than the underlying rock surface. A scanner or camera with multiple echo channels is expected to solve this issue (Xu et al. 2023).

Another significant challenge in slope stability evaluation is uncertainty. The rock mass itself exhibits considerable variability at different locations, and the parameters obtained from investigations are often discrete. The uncertainty in the internal structure and mechanical properties of the slope, along with the discrete and often sparse nature of the parameters derived from field investigations, complicates accurate stability assessments. These uncertainties can lead to significant variation in the predicted slope behavior, making it challenging to ensure reliable stability results using traditional deterministic approaches (Ng et al. 2021). While deterministic analysis can provide stability results within a certain range of parameters, as shown in Figures 12 and 13, it is primarily suited for engineering projects where parameter variations are relatively constant or uniform. Thus, it is crucial to employ suitable methods and tools to analyze slope failure behavior, such as probabilistic calculation methods that incorporate multiple uncertainties (Ng et al. 2021; Ng et al. 2022), and to identify potential failure mechanisms based on available data (Obregon and Mitri 2019; Zhang et al. 2022). Thus, it is crucial to employ methods that can address these uncertainties, such as probabilistic stability evaluation method. These methods integrate the spatial variability of rock mass properties, discontinuities, and mechanical behaviors, providing a more robust framework for predicting slope failure probabilities under uncertain conditions. For example, the probabilistic stability evaluation method, based on the spatial variability of discontinuities, has been employed by Matasci et al. (2018), who used statistical distributions of structural plane groups to analyze slope stability. Basahel and Mitri (2019) used the probability of structural plane intersections to analyze the sensitivity of falling blocks. Another approach involves the use of Discrete Fracture Networks (DFN), which are based on random simulations. To better capture the real slope conditions, comprehensive geological data on discontinuities is essential (Elmo and Stead 2010; Wang et al. 2023).

The slope surface is a critical parameter in rockfall simulations, and numerous studies have used 3D models to describe topography (Jiang et al. 2020). The proposed method allows for easy extraction of 3D variations in slope shape (e.g. ridges, convex talus cones, micro-topography), which significantly influence rockfall trajectories. These results can support the design of passive retaining structures. Other studies emphasize the need for long-term monitoring in areas with high rockfall hazard,

obtaining deformation and rock mass development data through time-interval observations to predict rock collapse timing (Li et al. 2020). The proposed method improves the range and accuracy of deformation, and the combination of temporal frequency monitoring with the parameters obtained in this study will be crucial for rockfall hazard assessment. Furthermore, for high and steep rock slopes like those at this quarry, monitoring data and stability estimation deliverables are essential not only for shallow support design but also for ensuring safety during slope excavation.

6. Conclusions

By fully utilizing geometric information alongside advanced investigation methods and field surveys, a stability estimation framework for shallow blocks located at high, steep slopes has been developed. This approach provides a more comprehensive stability analysis by combining new survey techniques with traditional methods. The proposed method leverages TLS and UAV photogrammetry to delineate precisely and visually unstable rock blocks, allowing for a better understanding of block failure mechanisms. The proposed method integrates on-site testing to determine the mechanical parameters of the blocks and a high-quality 3D model reconstruction to analyze block shapes and failure categories. This approach is adaptable to the complexities of mountainous and canyon terrain, enabling rapid geological data acquisition even in challenging conditions. Furthermore, it reduces fieldwork costs and hazards, enhances data acquisition speed and quality, and ensures high accuracy.

Soil filled fissure plays a significant role in block stability by reducing the cohesion between rock blocks, thereby increasing the likelihood of block detachment and failure. This highlights the complex nature of slope failure, where multiple factors, including soil properties and geological structures, interact to influence stability. However, with the proposed method, it is possible to generate a high-quality 3D model and conduct a detailed geological survey of rockfalls using point clouds obtained from TLS-UAV 3D data. The improved geometric characterization, including more accurate data on detachment locations, discontinuity orientations, block volumes, and failure mechanisms, enhances the ability to assess rockfall hazard and provides more reliable estimates of potential block detachment. This, in turn, supports more informed decisions on slope stabilization measures and hazard mitigation.

Acknowledgments

Critical comments by the anonymous reviewers greatly improved the initial manuscript.

Disclosure statement

No potential conflict of interest was reported by the author(s).

Funding

We gratefully acknowledge the support of the National Key R&D Program of China (2022YFC3080100), the National Natural Science Foundation of China (U2240221 and

42102316), and the Open Research Fund of the Key Laboratory of Reservoir and Dam Safety Ministry of Water Resources (YK323002).

References

- Abellán A, Vilaplana JM, Martínez J. 2006. Application of a long-range Terrestrial Laser Scanner to a detailed rockfall study at Vall de Núria (Eastern Pyrenees, Spain). *Eng Geol.* 88(3–4):136–148. doi: [10.1016/j.enggeo.2006.09.012](https://doi.org/10.1016/j.enggeo.2006.09.012).
- Badoux A, Andres N, Techel F, Hegg C. 2016. Natural hazard fatalities in Switzerland from 1946 to 2015. *Nat Hazards Earth Syst Sci.* 16(12):2747–2768. doi: [10.5194/nhess-16-2747-2016](https://doi.org/10.5194/nhess-16-2747-2016).
- Basahel H, Mitri HS. 2019. Probabilistic assessment of rock slopes stability using the response surface approach – A case study. *Int J Mining Sci Technol.* 29(3):357–370. doi: [10.1016/j.ijmst.2018.11.002](https://doi.org/10.1016/j.ijmst.2018.11.002).
- Blaszczyk M, Laska M, Sivertsen AH, Jawak SD. 2022. Combined use of aerial photogrammetry and terrestrial laser scanning for detecting geomorphological changes in Hornsund, Svalbard. *Remote Sens.* 14(3):601. doi: [10.3390/rs14030601](https://doi.org/10.3390/rs14030601).
- Cabo C, Sanz-Ablanedo E, Roca-Pardinas J, Ordóñez C. 2021. Influence of the number and spatial distribution of ground control points in the accuracy of UAV-SFM DEMs: an approach based on generalized additive models. *IEEE Trans Geosci Remote Sensing.* 59(12):10618–10627. doi: [10.1109/TGRS.2021.3050693](https://doi.org/10.1109/TGRS.2021.3050693).
- Chen J, Li H, Jiang N, Chen Q, Zhou J. 2024. A method for automatic assessment of rockfall susceptibility based on High-Resolution Point Clouds. *Rock Mech Rock Eng.* 57(3):1717–1733. doi: [10.1007/s00603-023-03651-2](https://doi.org/10.1007/s00603-023-03651-2).
- Cledat E, Jospin LV, Cucci DA, Skalous J. 2020. Mapping quality prediction for RTK/PPK-equipped micro-drones operating in complex natural environment. *ISPRS J Photogramm Remote Sens.* 167:24–38. doi: [10.1016/j.isprsjprs.2020.05.015](https://doi.org/10.1016/j.isprsjprs.2020.05.015).
- Copyright RIEGL Laser Measurement Systems GmbH. 2024. <http://www.riegl.com/index.php?id=221>.
- Damjanović V, Arbanas SM, Gazibara SB, Peranić J, Sećanj M, Krkač M, Arbanas Ž. 2020. Landslide mapping based on UAV photogrammetry using SFM—The Prnjavor Čuntićki Landslide Case Study, Croatia. In: Guzzetti F, Mihalić Arbanas S, Reichenbach P, Sassa K, Bobrowsky PT, Takara K, editors. *Understanding and reducing landslide disaster risk, WLF 2020, ICL contribution to landslide disaster risk reduction*. Cham: Springer; p. 95–101. doi: [10.1007/978-3-030-60227-7_9](https://doi.org/10.1007/978-3-030-60227-7_9).
- Elmo D, Stead D. 2010. An Integrated Numerical Modelling–Discrete Fracture Network approach applied to the characterisation of rock mass strength of naturally fractured pillars. *Rock Mech Rock Eng.* 43(1):3–19. doi: [10.1007/s00603-009-0027-3](https://doi.org/10.1007/s00603-009-0027-3).
- Ferrero AM, Forlani G, Roncella R, Voyat HI. 2009. Advanced geosurvey methods applied to rock mass characterization. *Rock Mech Rock Eng.* 42(4):631–665. doi: [10.1007/s00603-008-0010-4](https://doi.org/10.1007/s00603-008-0010-4).
- Gigli G, Lombardi L, Carlà T, Beni T, Casagli N. 2022. A method for full three-dimensional kinematic analysis of steep rock walls based on high-resolution point cloud data. *Int J Rock Mech Min Sci.* 157:105178. doi: [10.1016/j.ijrmms.2022.105178](https://doi.org/10.1016/j.ijrmms.2022.105178).
- Günther A, Carstensen A, Pohl W (. 2004. Automated sliding susceptibility mapping of rock slopes. *Nat Hazards Earth Syst Sci.* 4(1):95–102. doi: [10.5194/nhess-4-95-2004](https://doi.org/10.5194/nhess-4-95-2004).
- Hoek E, Bray JD. 1981. *Rock slope engineering*. London: CRC Press eBooks. doi: [10.1201/9781482267099](https://doi.org/10.1201/9781482267099).
- Jaboyedoff M, Chigira M, Arai N, Derron M, Rudaz B, Tsou C. 2019. Testing a failure surface prediction and deposit reconstruction method for a landslide cluster that occurred during Typhoon Talas (Japan). *Earth Surf Dynam.* 7(2):439–458. doi: [10.5194/esurf-7-439-2019](https://doi.org/10.5194/esurf-7-439-2019).
- Jiang N, Li H, Li C, Xiao H, Zhou J. 2022. A fusion method using terrestrial laser scanning and unmanned aerial vehicle photogrammetry for landslide deformation monitoring under complex terrain conditions. *IEEE Trans Geosci Remote Sensing.* 60:1–14. doi: [10.1109/TGRS.2022.3181258](https://doi.org/10.1109/TGRS.2022.3181258).

- Jiang N, Li H, Liu M, Zhang J, Zhou J. 2020. Quantitative hazard assessment of rockfall and optimization strategy for protection systems of the Huashiya cliff, southwest China. *Geomatics Nat Hazards Risk*. 11(1):1939–1965. doi: [10.1080/19475705.2020.1819445](https://doi.org/10.1080/19475705.2020.1819445).
- Lan H, Martin CD, Zhou C, Lim CH. 2010. Rockfall hazard analysis using LiDAR and spatial modeling. *Geomorphology*. 118(1–2):213–223. doi: [10.1016/j.geomorph.2010.01.002](https://doi.org/10.1016/j.geomorph.2010.01.002).
- Li C, Chen G, Guo L, Gao J, Peng X, Yu P. 2022. Slope stability and post-failure analysis of soil-rock-mixture using the modified 2D DDA-SPH method. *Int J Rock Mech Min Sci*. 157: 105170. doi: [10.1016/j.ijrmms.2022.105170](https://doi.org/10.1016/j.ijrmms.2022.105170).
- Li H, Li X, Li W, Zhang S, Zhou J. 2019. Quantitative assessment for the rockfall hazard in a post-earthquake high rock slope using terrestrial laser scanning. *Eng Geol*. 248:1–13. doi: [10.1016/j.enggeo.2018.11.003](https://doi.org/10.1016/j.enggeo.2018.11.003).
- Li H, Qi S, Yang X, Li X, Zhou J. 2020. Geological survey and unstable rock block movement monitoring of a Post-Earthquake high rock slope using terrestrial laser scanning. *Rock Mech Rock Eng*. 53(10):4523–4537. doi: [10.1007/s00603-020-02178-0](https://doi.org/10.1007/s00603-020-02178-0).
- Lian X, Li Z, Hong-Yan Y, Liu J, Zhang Y, Liu X, Yan-Ru W. 2020. Rapid identification of landslide, collapse and crack based on low-altitude remote sensing image of UAV. *J Mt Sci*. 17(12):2915–2928. doi: [10.1007/s11629-020-6080-9](https://doi.org/10.1007/s11629-020-6080-9).
- Markland JT. 1972. A useful technique for estimating the stability of rock slopes when the rigid wedge sliding type of failure is expected. Interdepartmental Rock Mechanics Project, Imperial College of Science and Technology, London.
- Matasci B, Stock GM, Jaboyedoff M, Carrea D, Collins BD, Guérin A, Matasci G, Ravelle L. 2018. Assessing rockfall susceptibility in steep and overhanging slopes using three-dimensional analysis of failure mechanisms. *Landslides*. 15(5):859–878. doi: [10.1007/s10346-017-0911-y](https://doi.org/10.1007/s10346-017-0911-y).
- Mavrouli O, Corominas J. 2017. Comparing rockfall scar volumes and kinematically detachable rock masses. *Eng Geol*. 219:64–73. doi: [10.1016/j.enggeo.2016.08.013](https://doi.org/10.1016/j.enggeo.2016.08.013).
- Ng CW, Qu C, Cheung RW, Guo H, Ni J, Chen Y, Zhang S. 2021. Risk assessment of soil slope failure considering copula-based rotated anisotropy random fields. *Comput Geotech*. 136:104252. doi: [10.1016/j.compgeo.2021.104252](https://doi.org/10.1016/j.compgeo.2021.104252).
- Ng CW, Qu C, Ni J, Guo H. 2022. Three-dimensional reliability analysis of unsaturated soil slope considering permeability rotated anisotropy random fields. *Comput Geotech*. 151: 104944. doi: [10.1016/j.compgeo.2022.104944](https://doi.org/10.1016/j.compgeo.2022.104944).
- Ng CW, Zhang Q, Ni J, Li Z. 2021. A new three-dimensional theoretical model for analysing the stability of vegetated slopes with different root architectures and planting patterns. *Comput Geotech*. 130:103912. doi: [10.1016/j.compgeo.2020.103912](https://doi.org/10.1016/j.compgeo.2020.103912).
- Obregon C, Mitri HS. 2019. Probabilistic approach for open pit bench slope stability analysis – A mine case study. *Int J Mining Sci Technol*. 29(4):629–640. doi: [10.1016/j.ijmst.2019.06.017](https://doi.org/10.1016/j.ijmst.2019.06.017).
- Puniach E, Gruszczynski W, Stoch T, Mrocheń D, Ćwiakała P, Sopata P, Pastucha E, Matwij W. 2023. Determination of the coefficient of proportionality between horizontal displacement and tilt change using UAV photogrammetry. *Eng Geol*. 312:106939. doi: [10.1016/j.enggeo.2022.106939](https://doi.org/10.1016/j.enggeo.2022.106939).
- Riquelme A, Abellán A, Tomás R, Jaboyedoff M. 2014. A new approach for semi-automatic rock mass joints recognition from 3D point clouds. *Computers Geosci*. 68:38–52. doi: [10.1016/j.cageo.2014.03.014](https://doi.org/10.1016/j.cageo.2014.03.014).
- Šašak J, Gallay M, Kaňuk J, Hofierka J, Minár J. 2019. Combined use of terrestrial laser scanning and UAV photogrammetry in mapping alpine terrain. *Remote Sens*. 11(18):2154. doi: [10.3390/rs11182154](https://doi.org/10.3390/rs11182154).
- Siqueira H, Marcato J, Matsubara ET, Eltner A, Colares RA, Santos FM. 2019. The impact of ground control point quantity on area and volume measurements with UAV SFM photogrammetry applied in open pit mines. *IEEE International Symposium on Geoscience and Remote Sensing*, p. 9093–9096. doi: [10.1109/igarss.2019.8897829](https://doi.org/10.1109/igarss.2019.8897829).
- Wang G, Zhao B, Wu B, Zhang C, Liu W. 2023. Intelligent prediction of slope stability based on visual exploratory data analysis of 77 in situ cases. *Int J Mining Sci Technol*. 33(1):47–59. doi: [10.1016/j.ijmst.2022.07.002](https://doi.org/10.1016/j.ijmst.2022.07.002).

- Wang M, Zhou J, Chen J, Jiang N, Zhang P, Li H. 2023. Automatic identification of rock discontinuity and stability analysis of tunnel rock blocks using terrestrial laser scanning. *J Rock Mech Geotech Eng.* 15(7):1810–1825. doi: [10.1016/j.jrmge.2022.12.015](https://doi.org/10.1016/j.jrmge.2022.12.015).
- Xu Q, Zhao B, Dai K, Dong X, Li W, Zhu X, Yang Y, Xiao X, Wang X, Jian H, et al. 2023. Remote sensing for landslide investigations: a progress report from China. *Eng Geol.* 321: 107156. doi: [10.1016/j.enggeo.2023.107156](https://doi.org/10.1016/j.enggeo.2023.107156).
- Zhang W, Li H, Han L, Chen L, Wang L. 2022. Slope stability prediction using ensemble learning techniques: a case study in Yunyang County, Chongqing, China. *J Rock Mech Geotech Eng.* 14(4):1089–1099. doi: [10.1016/j.jrmge.2021.12.011](https://doi.org/10.1016/j.jrmge.2021.12.011).
- Zhou J, Chen J, Li H. 2024b. An optimized fuzzy K-means clustering method for automated rock discontinuities extraction from point clouds. *Int J Rock Mech Min Sci.* 173:105627. doi: [10.1016/j.ijrmms.2023.105627](https://doi.org/10.1016/j.ijrmms.2023.105627).
- Zhou J, Jiang N, Li H. 2024a. Automatic discontinuity identification and quantitative monitoring of unstable blocks using terrestrial laser scanning in large landslide during emergency disposal. *Landslides.* 21(3):607–620. doi: [10.1007/s10346-023-02169-6](https://doi.org/10.1007/s10346-023-02169-6).